Analysis of asphaltenes and maltenes before and after long-term aging of bitumen

Analysis of asphaltenes and maltenes before and after long-term aging of bitumen

Xiaohu Lu [a *], Hilde Soenen [b], Peter Sjövall [c], Georgios Pipintakos [d]

[a] Nynas AB, SE 149 82, Nynäshamn, Sweden

[c] Nynas NV, 2020 Antwerp, Belgium

[b] RISE Research Institutes of Sweden, SE 501 15, Borås, Sweden

[d] University of Antwerp, 2020 Antwerp, Belgium

Corresponding author: xiaohu.lu@nynas.com

Abstract

Asphaltenes and maltenes of bitumen before and after aging are investigated by differential scanning calorimetry (DSC), Fourier transform infrared spectroscopy (FTIR), proton nuclear magnetic resonance spectroscopy (^{1}H-NMR), time of flight - secondary ion mass spectrometry (TOF-SIMS), and gel permeation chromatography (GPC). It has been shown that bitumen differs in terms of wax. After fractionation, more wax is found in the maltenes compared to the bitumen, and this is even more evident when bitumen is aged. For one bitumen, asphaltenes from the virgin binder do not contain carbonyls, which all fall into the maltenes. After bitumen aging, a large part of the carbonyl and sulfoxide signals is shifted to the asphaltenes. Differences in aromaticity are also evidenced as asphaltenes > bitumen > maltenes. TOF-SIMS shows that maltenes are close to the bitumen, but asphaltenes are more different. Also, maltenes are relatively unaffected by aging while larger differences are found in the asphaltenes between the virgin and aged binders. By GPC, a large molecular weight fraction of bitumen is shown as main part of the asphaltenes. However, asphaltenes also contain low molecular weight molecules that overlap with maltenes. Upon bitumen aging, some low molecular weight compounds may become part of asphaltenes, making the average molecular weight of the asphaltenes lower.

Keywords: Bitumen, Asphaltenes, Maltenes, Aging, Chemical analysis

1. Introduction

Produced from certain crude oils, bitumen consists of large number of organic compounds differing in molecular structure, molecular weight, and polarity. To make a chemical characterization and to

investigate the relationships between chemistry and mechanics, bitumen is often fractionated according to standard procedures, such as ASTM D 3279 [1], ASTM D 4124 [2], IP 143 [3], and IP 469 [4]. Commonly, by using n-heptane as a solvent, bitumen is first separated into two fractions, asphaltenes and maltenes, defined as n-heptane insoluble (and toluene soluble) fraction and n-heptane soluble fraction, respectively. For maltenes, further separation can be made to obtain saturates, aromatics, and resins. It should be noticed that the fractionation of bitumen may be also performed using another defined hydrocarbon n-pentane, and the obtained asphaltenes and maltenes are not the same as those by n-heptane.

Asphaltenes and maltenes of bitumen have been investigated extensively over the years. Research focus is not only on the chemistry of these fractions but also on their impacts on the mechanical and rheological properties of bitumen. As a solubility class of hydrocarbon components, asphaltenes consist of a complex mixture of many compounds, containing the molecules of bitumen with the strongest dispersive interactions as well as the strongest π - π interactions [5]. In general, asphaltenes are a fraction of relatively large molecules of bitumen. The average molecular weight of asphaltenes is roughly 750 g/mole, within a range of 300 to 1400 g/mol [6]. Dominantly, there is one polycyclic aromatic hydrocarbon (PAH) core per asphaltene molecule, and asphaltene PAHs have 4 to 10 fused rings [6]. Depending on the chemical nature, asphaltene molecules can aggregate in maltenes or bitumen [7-9], thus making the molecular weight of asphaltenes apparently higher. The aggregation of asphaltenes can be driven by several intermolecular forces, including π-stacking of aromatic cores, London dispersion forces between aliphatic moieties, hydrogen bonding between nitrogen and oxygen-containing functionalities, and acid/base interactions between carboxylic acids and pyridine rings [10].

Historically, bitumen is described as a colloidal system with dispersions of asphaltenes in maltenes [11-13]. The colloidal model was used to explain the material's Newtonian and non-Newtonian rheological behavior [14-16]. By a systematic blending of bitumen generic fractions, asphaltenes were demonstrated to be responsible for the high viscosities and non-Newtonian rheological properties of bitumen [17, 18]. Also, by remixing different weight ratios of the asphaltenes and the maltenes obtained from different source bitumen, the binders' characteristic microstructures were found to correlate with their bulk thermal and mechanical properties [19]. It has also been shown that, among different fractions, asphaltenes display the lowest temperature susceptibility [17, 20, 21], and significantly contribute to bitumen's stiffness, rigidity, and elasticity [22-25]. On the other hand, for a better fatigue resistance, limiting the contents of asphaltenes in the bitumen would be helpful [26]. In a study conducted during the Strategic Highway Research Program (SHRP), the thickening effect of asphaltenes was examined in a set of bitumen produced from different crude oils

using different techniques [27]. By defining a relative viscosity of bitumen as the quotient of the viscosity of the whole bitumen divided by the viscosity of the n-heptane soluble maltene fraction at a given temperature and rate of shear, compatibility of the bitumen was also examined. Evidently, a deep understanding of asphaltenes and maltenes is essential to establish the relationships between bitumen chemistry and rheology.

Understanding the chemistry of asphaltenes and maltenes is also of great importance to asphalt recycling or rejuvenation of reclaimed asphalt pavement (RAP). In ref [28], it was found that the most notable changes upon the oxidative aging occur in the asphaltenes, as well as in aromatics and resins; the formation of carbonyls can be tracked in all these three fractions, while the formation of sulfoxides is found in the asphaltenes and resins. It was also reported that the aging-induced chemical changes vary with the aging methods and the crude oil sources for bitumen [29]. In ref [30], an automated asphaltene determinator coupled with saturates, aromatics, and resins separation (SAR-AD) has been developed for characterization of petroleum materials. By the SAR−AD method, the most polar and pericondensed asphaltenes as a result of thermal cracking as well as other diagnostic compositional changes during the oxidative aging were quantified [31]. In ref [32], laboratory aging was performed on various blends of asphaltenes and maltenes (prepared using n-hexane) from different SHRP asphalt binders, as well as on maltenes and some parent binders. It was reported that the oxidative aging of bituminous binders and maltenes results in the formation of carbonyl compounds, the production of asphaltenes, and an increase in viscosity. It was also found that the maltene composition has the dominant effect on the oxidation behavior of the binders. This would suggest that a recycling agent (or rejuvenator) for RAP should be chosen properly to ensure good oxidation properties for the mixture of the recycling agent and the maltenes from the RAP. A good rejuvenator should also be able to restore the properties of a RAP binder through readjusting the balance between the asphaltene and maltene fractions [33]. Moreover, according to molecular dynamics simulation, a good recycling agent is effective in the deagglomeration of oxidized asphaltenes [34].

The main objective of this study is to chemically investigate asphaltenes and maltenes of bitumen, especially, to investigate how these fractions change upon the oxidative aging of the bitumen. For this purpose, laboratory long-term aging was performed on selected bitumen samples, followed by fractionation of the binders according to a standard procedure. For chemical analysis, various techniques were used, including Fourier transform infrared spectroscopy (FTIR), nuclear magnetic resonance spectroscopy (^{1}H-NMR), time of flight - secondary ion mass spectrometry (TOF-SIMS), and gel permeation chromatography (GPC). For comparison, all the chemical analyses were also carried out on virgin and aged bitumen samples.

2. Experimental section

2.1 Bitumen samples

Two bitumen samples, coded as B25 and B26, respectively, were investigated. The bitumen samples have an identical penetration grade of 160/220, but they differ in chemical compositions and structures [35]. The samples were aged by Rolling Thin Film Oven Test (RTFOT, EN 12607-1) [36] followed by Pressure Aging Vessel (PAV, EN 14769) at 100°C for 20 hours (i.e. long-term aging) [37]. Properties and compositions of the binders before and after the laboratory long-term aging are shown in Table 1. In Table 1, the elemental compositions were measured according to ASTM D 5291 [38], and SARA (saturates, aromatics, resins and asphaltenes) analysis was performed by thin-layer chromatography with flame ionization detection (TLC-FID) according to IP 469 [4].

2.2 Fractionation of bitumen

Fractionation of bitumen into asphaltenes and maltenes was carried out on the virgin and the RTFOT+PAV aged binders. This was performed basically according to DIN 51595 [39], which is technically identical to IP 143 [3]. About 60 g of hot bitumen was poured into an Erlenmeyer flask, then n-heptane solvent was added in the ratio of 100 mL of solvent per 1 g of sample. With slightly heating on a hot plate, the Erlenmeyer flask was shaken until all the bitumen was partially dissolved and the other part was precipitated. After being rested for about a half hour, the solution with the precipitates (asphaltenes) was cooled to room temperature. Then a first filtration was performed on a Whatman 41 filter paper. The asphaltenes on the filter paper were washed repeatedly with the hot solvent until the filtrate was colorless. After drying the filter paper, the precipitates were collected in a beaker. The dried asphaltenes were washed one more time with n-heptane and filtered on a vacuum filter. Maltenes fraction was also collected from all n-heptane solutions after removing the solvent by a rotary rotavapor.

Table 1. Properties of bitumen samples before and after long-term aging

	B25		B26	
	Virgin	Aged	Virgin	Aged
Penetration, 1/10 mm	187	63	190	26
Softening point, °C	39.6	50.0	39.2	69.0
Elemental compositions, %				
Carbon	85.6	85.2	85.2	85.5
Hydrogen	10.6	10.5	9.9	9.8
Nitrogen	0.5	0.5	0.5	0.5
Sulfur	3.3	3.2	3.9	3.9
Oxygen	0.5	1.0	0.1	1.0
SARA fractions, %				
Saturates	7.6	7.7	5.6	5.5
Aromatics	44.4	35.7	50.3	37.6
Resins	23.2	32.0	22.9	30.9
Asphaltenes	21.8	24.6	21.2	25.9

2.3 Analytical methods

2.3.1 Differential scanning calorimetry (DSC)

DSC analysis was carried out with a Mettler Toledo DSC1 under N_2 atmosphere. To avoid pressure build-up, sample holders with a small hole were used. A sample was first heated to 140°C and kept at this temperature for about 10 min. The data were recorded during cooling to –65°C, followed by heating to 140°C. Both the heating and cooling rates were 10°C/min. The measured thermal characteristics include glass transition temperature (Tg) and enthalpy for wax melting.

2.3.2 Fourier transform infrared spectroscopy (FTIR)

FTIR with attenuated total reflection (ATR) was performed using a Nicolet IS 10 with a diamond cell (smart-orbit). In FTIR-ATR, a very small amount of sample was directly placed on an ATR crystal and IR reflection from the sample was measured. Spectra were recorded at wavelengths ranging from 600 to 4000 cm^{-1}, which characterize different functional groups, such as carbonyl compounds at around 1700 cm^{-1}, sulfoxide at about 1030 cm^{-1}, as well as aromaticity at 1600 cm^{-1}. For the sample preparation, bitumen and maltenes were heated for about 15 minutes at 160°C and 120°C respectively in small metal containers in order to obtain a liquid state. All the samples were properly stirred with a metal spoon before the analysis to let any remaining voids escape and ensure a homogeneous sample. Finally, a hot droplet was placed on the crystal and was let to cool down

before the spectrum acquisition. It should be noted that any additional oxidation that can be induced by sample storage was limited by storing all the samples in dark and was compensated by this homogenization stirring. As for asphaltenes, powder sample was taken from a sealed black box.

2.3.3 Proton nuclear magnetic resonance spectroscopy (^{1}H-NMR)

In ^{1}H-NMR, data collection was conducted at room temperature with a high-resolution liquid-state Bruker Avance III HD 400 MHz smart probe spectrometer (32 scans), 30-degree excitation pulse. 20 mg of sample were dissolved in 550 µl of deuterated tetrachloroethane ($C_2D_2Cl_4$) inside borosilicate NMR tubes (ASTM Type 1 Class B glass) of diameter 5 mm and a wall thickness of 0.4 mm. The exact mass of the samples was measured beforehand and was placed in vials at room temperature. The samples were heated shortly in a bath at 40°C to ensure a homogeneous solution and finally placed in an ultrasonic bath for 1 minute prior to ^{1}H-NMR measurements.

The above ^{1}H-NMR sample preparation was used for bitumen and maltenes, but it was unsuccessful for asphaltenes. Prior trials to dissolve asphaltenes failed although the temperature and dissolution time were considerably increased to obtain a homogeneous solution. Asphaltene particles were still visible and as such no ^{1}H-NMR measurements were carried out due to a risk of high variability between replicates or misinterpretation of the obtained spectra.

2.3.4 Time of flight - secondary ion mass spectrometry (TOF-SIMS)

In TOF-SIMS, collisions of primary ions with the sample surface result in the emission of a variety of particles, including atoms, molecular fragments, intact molecules, and molecular complexes. Most of these particles are neutral but a small fraction comes off as ions. The emitted (secondary) ions, which can be either positive or negative, are analyzed in a TOF analyzer. For TOF-SIMS analysis, powder samples of asphaltenes were attached on separate silicon substrates using double-sided tape. The maltene and bitumen samples were deposited as ca 0.5-1 mm thick films on carefully cleaned silicon substrates according to the following procedure: after heating the maltene/bitumen in an oven at 130 °C for 1 hour, a droplet of the sample was placed on the silicon substrate using a glass pipette. The sample was again briefly heated to 130 °C, then allowed to cool slowly to room temperature during about 1 hour, whereafter it was placed in a freezer at -20 °C for about 1 hour. Finally, the sample was rapidly warmed up to room temperature, mounted on the sample holder and placed in the load lock of the TOF-SIMS instrument, where it was cooled down to -80 °C prior to evacuation and transfer into the analysis chamber. The analyses were carried out at a sample temperature of -80 °C to avoid migration and evaporation of the sample in the instrument vacuum chamber.

All the analyses were conducted on a TOF-SIMS IV instrument manufactured by ION-TOF GmbH (Münster, Germany) using 25 keV Bi_3^+ primary ions. Data for positive and negative ions were acquired

in static SIMS mode with the instrument optimized for high mass resolution and for high image resolution (separate measurements). Low energy electron flooding was used to compensate for sample charging during the analysis. Principal components analysis (PCA) of the TOF-SIMS data was carried out using the Solo software (version 7.8.2, Eigenvector Research, Inc, USA). PCA of the positive ion data included 295 selected peaks corresponding to hydrocarbon ions $C_xH_y^+$, with x=2-21 and y=1-24. For negative ion data, the PCA included nominal mass signal intensities at m/z=20-200. Prior to PCA, the peak intensities were normalized to the total signal intensity of all included ions/nominal mass values and pretreatment included Poisson scaling and mean centering.

2.3.5 Gel permeation chromatography (GPC)

GPC is a common technique to measure molecular weight. In this study, an Alliance 2690 Separation Module (Waters) with a refractive index detector was employed. The GPC columns used were two PL gel 5 μm MIXED-D columns (300mm x 7.5mm). As a mobile phase, tetrahydrofuran (THF) was chosen. This solvent was also used to prepare sample solutions of 0.4 w%. Calibration was carried out with polystyrene standards of known molecular weights. The obtained parameters include the number average molecular weight (Mn), the weight average molecular weight (Mw), as well as polydispersity index, Mw/Mn, which is a measure for the width of the molecular weight distribution.

3. Results and discussion

3.1 DSC

DSC has been widely applied to characterize the thermal properties of bitumen and its fractions [40, 41]. In DSC, curves of heat flow versus temperature provide insight into the thermal characteristics of bituminous materials, such as wax crystallization / melting [40-43] and glass transition temperature (Tg). Typical DSC diagrams are shown in Figure 1 for bitumen B26 and its maltene fraction; no results are shown for asphaltenes since asphaltenes were not melted under the testing conditions. In the heating scan, an endothermic reaction occurs, which is interpreted as melting of the wax. Thus, the melting enthalpy is a measurement of the wax present in the sample. As indicated in Figure 1, B26 and its maltene fraction display a similar melting starting temperature of slightly above -15°C, but they differ in melting out temperatures (about 90°C for B26 and 80°C for the maltenes). It is obvious that the melting takes place during a range of temperatures, indicating the presence of molecules with different melting points. The melting of a given molecule also depends on the surrounding chemical compositions, and this is the case when comparing the bitumen and the maltene fraction. On the other hand, the wax melting starting temperature and melting out temperature are apparently not affected by aging.

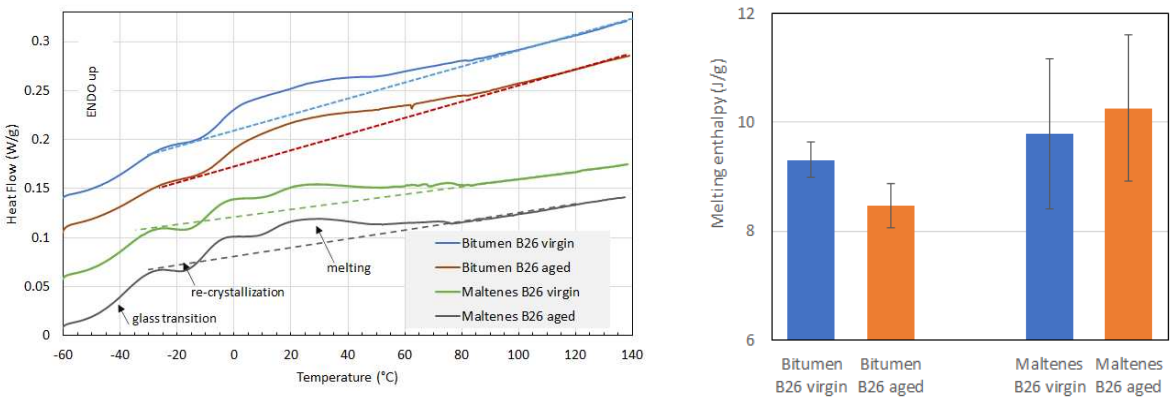

Figure 1. DSC thermograms (left) and melting enthalpies (right) for bitumen B26 and the maltenes from B26 before and after aging, heating scans at 10°C/min

Regarding melting enthalpy (Figure 1), the maltene fraction shows a higher value than the corresponding bitumen. Figure 1 also shows that, after the long-term aging, the malting enthalpy of the bitumen becomes lower, while for the maltenes the effect of aging is likely opposite. These results suggest that for the bitumen investigated, more wax is present in the maltenes when the bitumen is fractionated, especially after the long-term aging. As for bitumen B25, as well as its maltene fraction, no wax crystallization and melting were detected by DSC (thermograms not shown). This indicates that B25 is a wax-free bitumen.

3.2 FTIR

The IR spectra of asphaltenes and maltenes, as well as of their parent bitumen samples, are shown in Figure 2. The effect of aging on the bitumen is somewhat as expected. Increases are mainly seen in carbonyl and sulfoxide signals at 1700 cm^{-1} and 1030 cm^{-1}, respectively, and there is also a minor increase in aromaticity at 1600 cm^{-1}. The spectra also show that B25 already has a carbonyl signal in the unaged state. This is related to the fact that this binder is produced from an acid crude oil or a crude with a high acidity.

For asphaltenes, the IR spectra are obviously different from the bitumen samples and maltenes. The signals associated with the stretching or bending vibrations of saturated hydrocarbons at about 2920 cm^{-1}, 2850 cm^{-1}, 1460 cm^{-1} and 1376 cm^{-1} are different from those for the binders. For B26, it is also clear that in the unaged state, the asphaltenes do not contain carbonyls, which all fall into the maltene fraction. After aging, the asphaltenes contain a large part of the carbonyl and sulfoxide signals, suggesting that a lot of molecules become insoluble in warm n-heptane after they have reacted with oxygen to form carbonyl and sulfoxide groups. This is the case for both binders and can

explain the increase of the more polar fractions in asphaltenes due to aging. The observation is in agreement with that made by Mirwald et al. [29].

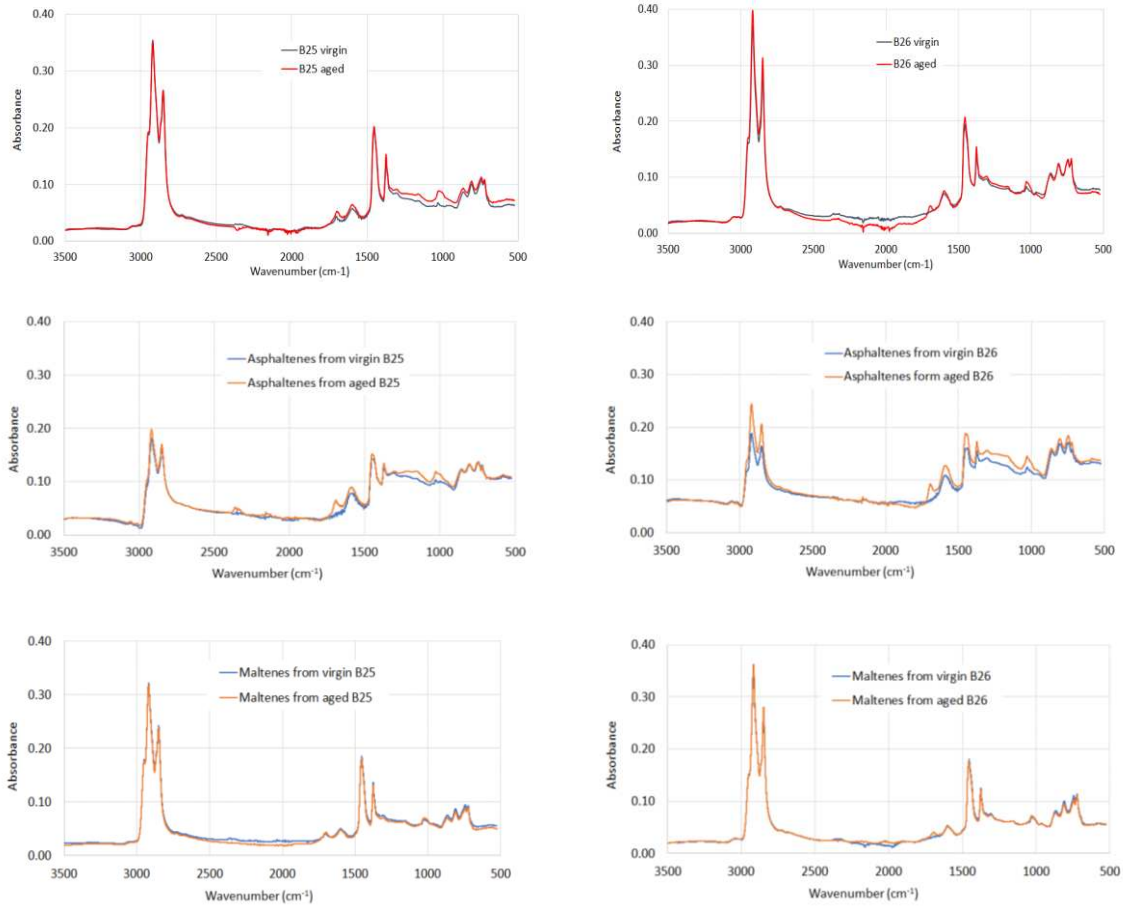

Figure 2. IR raw spectra of bitumen, asphaltenes and maltenes before and after aging

From Figure 2, one can also see that maltenes display raw spectra very similar to that of the parent bitumen. For unaged B26, as already discussed, the carbonyl signal is present in the maltene fraction, but not in the asphaltene fraction. It seems that these carbonyls are soluble in warm n-heptane. In general, for bitumen B25, the effect of aging on the maltene fraction as shown by IR is rather small. On the other hand, for B26, maltenes of the virgin binder contain a small part of carbonyls which is more pronounced than B25 upon aging.

Differences between the bitumen fractions and effects of aging are further shown by normalized peak areas in Figure 3. For the normalization of the FTIR spectra, the procedure described in [44] was adopted. For this procedure, first, all the spectra are shifted to zero absorbance at a fixed wavenumber of the lowest absorbance. Then an absorbance correction factor is applied to scale the spectra at the asymmetric stretching vibration of the aliphatic structures at 2923 cm^{-1}. The entire

spectrum is then multiplied by this ratio factor. Due to the considerable differences of the symmetric and asymmetric bending vibrations of the aliphatic groups at 1460 cm^{-1} and 1376 cm^{-1} for the different fractions, the normalized areas were preferred to be used instead of commonly used indices for a fair comparison. Besides those observations already made on carbonyls and sulfoxides, obvious difference is also shown by aromaticity (A1600), being ranked as asphaltenes > bitumen > maltenes. After aging, aromaticity is increased in the asphaltenes (and bitumen), but not in the maltenes.

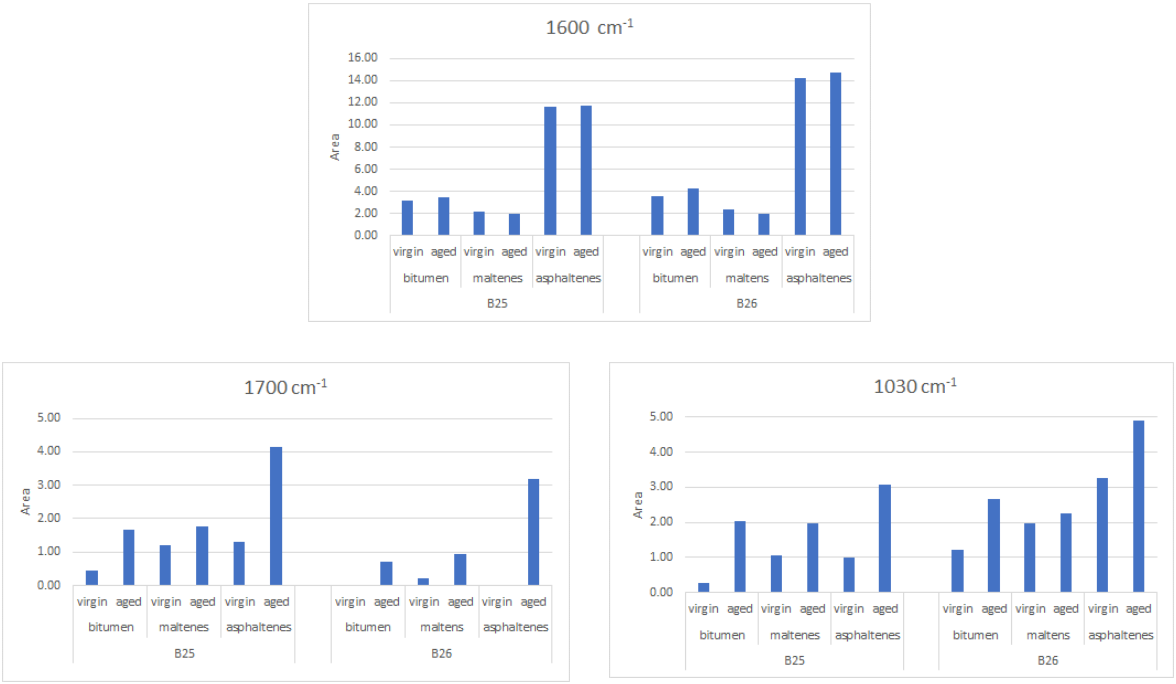

Figure 3. Normalized absorbance peak areas of different functional groups in bitumen, asphaltenes and maltenes before and after aging

3.3 ^{1}H-NMR

Examples of ^{1}H-NMR spectra are shown in Figure 4. In calculation, all spectra were first corrected for their baseline using the MestreNova spectral analysing software. The starting chemical shift based on the difference of the residue solvent peak (6.00 ppm) with respect to TMS (tetramethylsilane) (0.00 ppm) was defined. Integrations of the typical proton chemical shift regions given in Table 2 were performed for all the samples based on a previous study for bituminous samples [45]. The residue solvent peak at 6.00 ppm was omitted from the integrations. Normalization of all the integrated areas with the exact sample mass was carried out. The changes of the relative percentage changes do not always agree with the non-normalized integrations. However, the relative percentage distribution is rather consistent, free of mass-dependency, thus is chosen for the analysis.

In Figure 5, the relative hydrogen percentage distributions of different types of protons (methyl, methylene, α-alkyl, olefinic, aromatic) are plotted as the average of the two replicates with their standard deviation. The percentage distributions are shown for the maltenes, as well as for the corresponding bitumen before and after aging. No results are shown for asphaltenes since this fraction was not completely dissolved in deuterated tetrachloroethane (c.f. Section 2.3.2). Figure 5 indicates that the hydrogen percentage distributions are quite different in the maltene fractions. The maltenes from bitumen B25 show higher methyl region, lower α-alkyl region and lower aromatic region compared to the maltenes from B26. The differences between the maltenes fractions can already be seen from the two bitumen samples (Figure 5), possibly indicating that the binders were produced from different crude sources and/or by different refining processes. Figure 5 also shows that aging affects in a similar manner the two maltene fractions and the two bitumen samples, i.e. an increase is observed for methyl and methylene regions and a decrease seems to hold for aromatic and α-alkyl regions. In all the cases, the olefinic region is negligible. The changes upon aging are more obvious for the maltene fraction of B26 as compared to that of B25. This is also the case when the two bitumen samples are compared.

Table 2. Typical proton chemical shift regions

Designation	Chemical shift range	Type of protons
H_{methyl}	0.5-1.0	Aliphatic hydrogen on C_γ and the CH_3 beyond the C_γ to aromatic rings
$H_{methylene}$	1.0-2.0	Aliphatic hydrogen on C_β and the CH_2 beyond the C_β to aromatic rings
$H_{\alpha\text{-}alkyl}$	2.0-4.0	Aliphatic hydrogen on C_α to aromatic rings
$H_{olefinic}$	4.0-6.0	Olefinic hydrogen
$H_{aromatic}$	6.0-9.0	Aromatic hydrogen

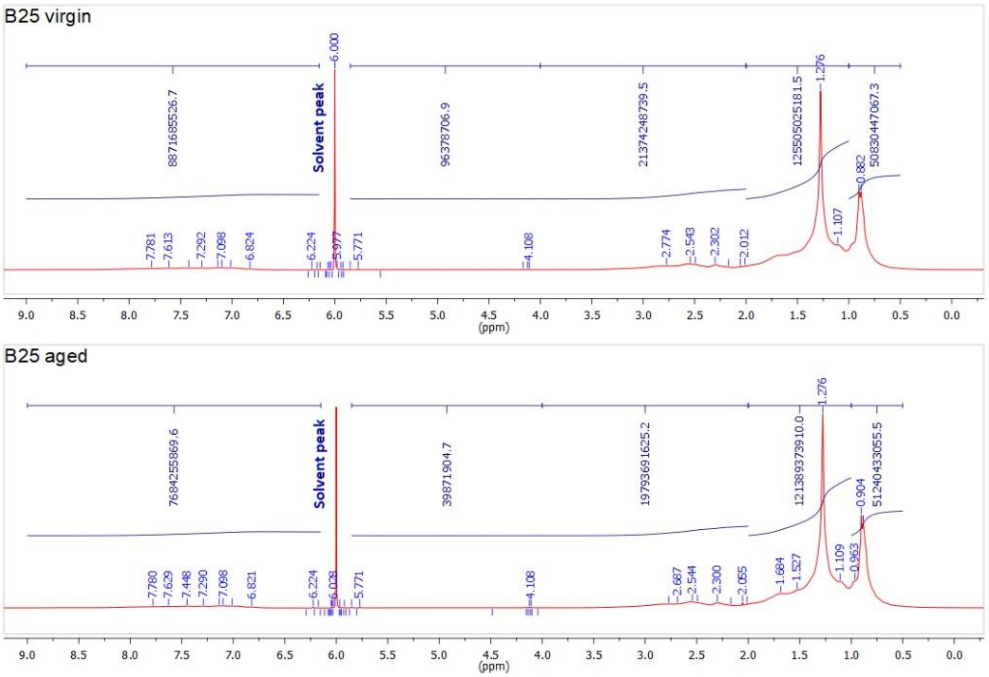

Figure 4. Examples of ^{1}H-NMR spectra for the maltenes from bitumen B25 (upper – virgin; lower – aged)

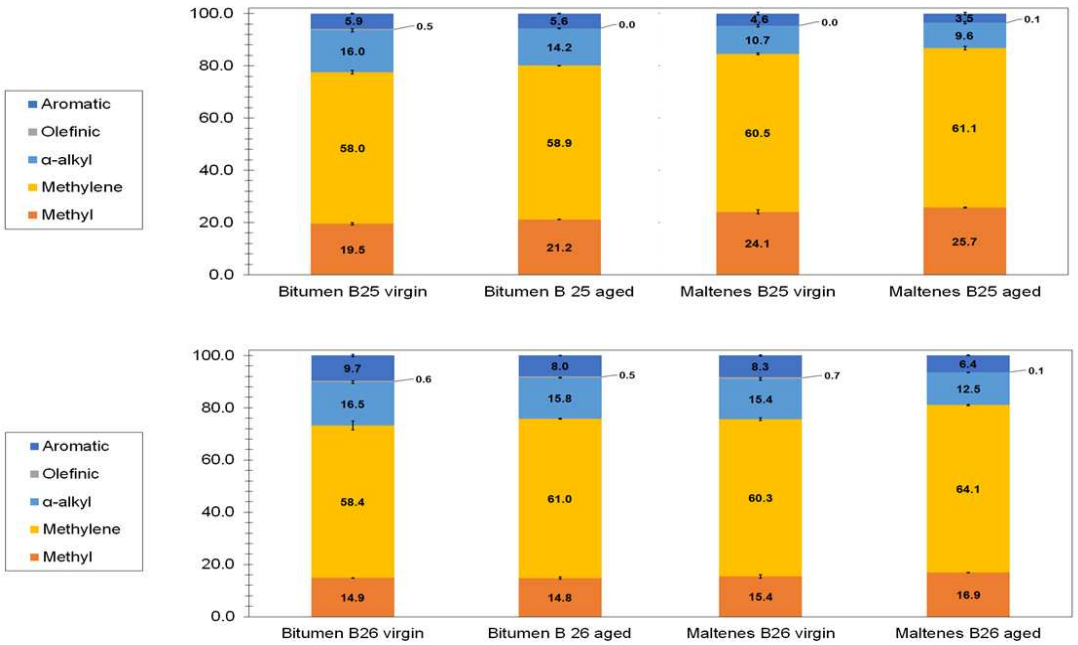

Figure 5. Relative hydrogen percentage distributions in bitumens and maltenes and effect of aging

3.4 TOF-SIMS

In TOF-SIMS, molecular information is obtained by irradiating the sample surface with a focused, high-energy primary ion beam and analyzing the emitted secondary ions with respect to mass.

Identification of the secondary ions (either positive or negative) in the acquired mass spectrum allows for association of individual peaks to specific molecular species on the sample surface. For bitumen samples, the positive ion spectra are dominated by peaks corresponding to hydrocarbon ions, $C_xH_y^+$, whereas the negative spectra display considerable peak intensities from heteroatom-containing ions as well as (hydrogen-deficient) hydrocarbon ions [35, 46].

To identify and characterize chemical differences between the asphaltenes, maltenes and bitumen, and to investigate aging effects, the TOF-SIMS spectra were evaluated by principal components analysis (PCA). For positive ions, signal intensities of 295 selected peaks, corresponding $C_xH_y^+$ ions (x=2-21, y=1-24), were used as input data to generate principal components (PCs), which are formed by combinations of peaks that vary in correlated manner between the spectra. The results of the PCA of the positive ions are shown in Figure 6, where the score plot (Figure 6A) indicate spectral similarities/differences between the samples, and the loadings (Figure 6B) specify the contribution of each peak to the principal component. Thus, the relative proximity of the maltene spectra with those of the corresponding bitumens in the score plot indicate a high degree of spectral similarity, whereas the asphaltenes are more different (note that separations along the horizontal (PC1) axis represent larger spectral differences than separations along the vertical (PC2) axis). Furthermore, the maltenes and bitumens are relatively unaffected by aging, whereas larger differences are found between the virgin and aged asphaltenes. Finally, clear differences are observed between B25 and B26, both for the maltenes and the asphaltenes.

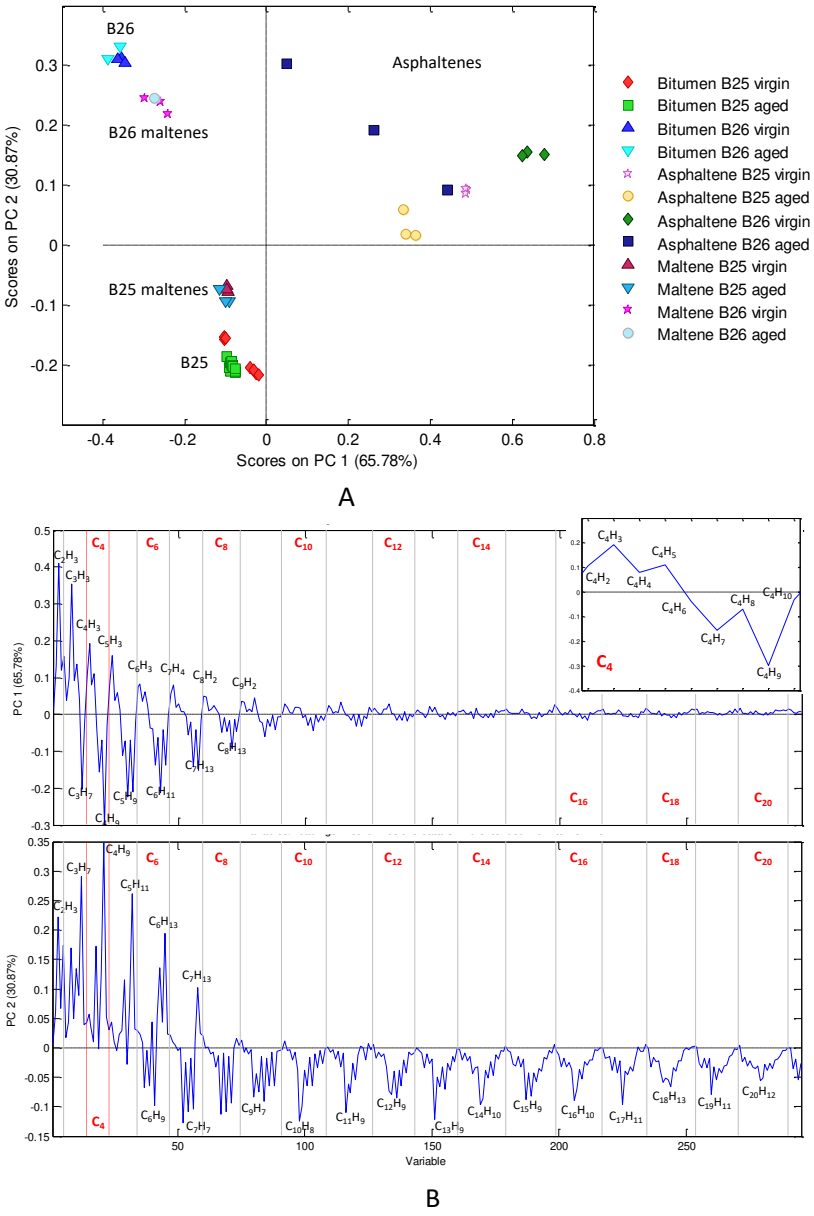

Figure 6. PCA analysis of positive TOF-SIMS spectra. (A) score plot displaying PC1 (horizontal) and PC2 (vertical) scores of spectra from the indicated samples. The percentages in the axis labels specify the explained variation, and thus the spectral differences represented, in each PC. (B) PC1 (upper) and PC2 (lower) loadings for the 295 included peaks/$C_xH_y^+$ ions. The peaks are arranged horizontally in groups with increasing x (separated by grey lines and indicated in red) and with increasing y within each group. As an example, the inset displays PC1 loadings of the $C_4H_y^+$ ions (x=4, y=2-10), highlighting a common pattern for all x, with positive loadings for low y and negative loadings for high y. In the lower diagram, the labelled ions with negative PC2 loadings correspond to characteristic PAH ions [47, 48].

The loadings in Figure 6B explain the spectral differences observed in the score plot in terms of the original peaks/ions, such that peaks with positive loadings are particularly strong in spectra with positive scores (for each PC) and peaks with negative loadings are particularly strong in spectra with negative scores. Interestingly, the PC1 loadings are consistently high/positive for ions with low H/C ratios (representing aromatic structures) and low/negative for ions with high H/C ratios (aliphatic structures). Thus, the high PC1 scores for the asphaltene spectra indicate a higher aromatic content as compared to the maltenes. Furthermore, positive PC2 loadings for aliphatic ions and negative loadings for characteristic PAH ions indicate higher aliphatic content in B26, as compared to B25. However, these systematic trends need to be verified by analysis of the actual peak intensities (Figure 7).

In Figure 7, the added signal intensities of selected aromatic, PAH, and aliphatic ions in the positive TOF-SIMS spectra are presented for the asphaltenes, maltenes, as well as for the corresponding bitumen. It is evident that asphaltenes are more aromatic (and less aliphatic) than bitumen and maltenes, as indicated in the PCA results. This agrees with the observation from FTIR. Upon aging of the bitumen, the asphaltene fractions show a decrease in the yields of aromatic ions and an increase in aliphatic ions. This could be a result of oxidized structures increasingly contributing to the asphaltene fraction after bitumen aging. Figure 7 also confirms that the maltenes from the wax-containing bitumen B26 are more aliphatic (and less aromatic) as compared to the maltenes from the non-waxy bitumen B25. The observed differences between the maltenes are already reflected in the bitumen samples, where B26 is more aliphatic (and less aromatic) than B25. As for PAH ions, the maltene fraction from B25 shows considerably higher signals than maltene from B26, and this is also the case when comparing bitumen B25 and B26. For the asphaltenes, differences in the PAH signal intensities between B25 and B26 are found to be smaller. Furthermore, PAH ions are very little affected by aging. It should be noted that $C_xH_2^+$ ions are characteristic for aromatic structures, whereas PAH ions are actually less characteristic of aromatic structures only [49].

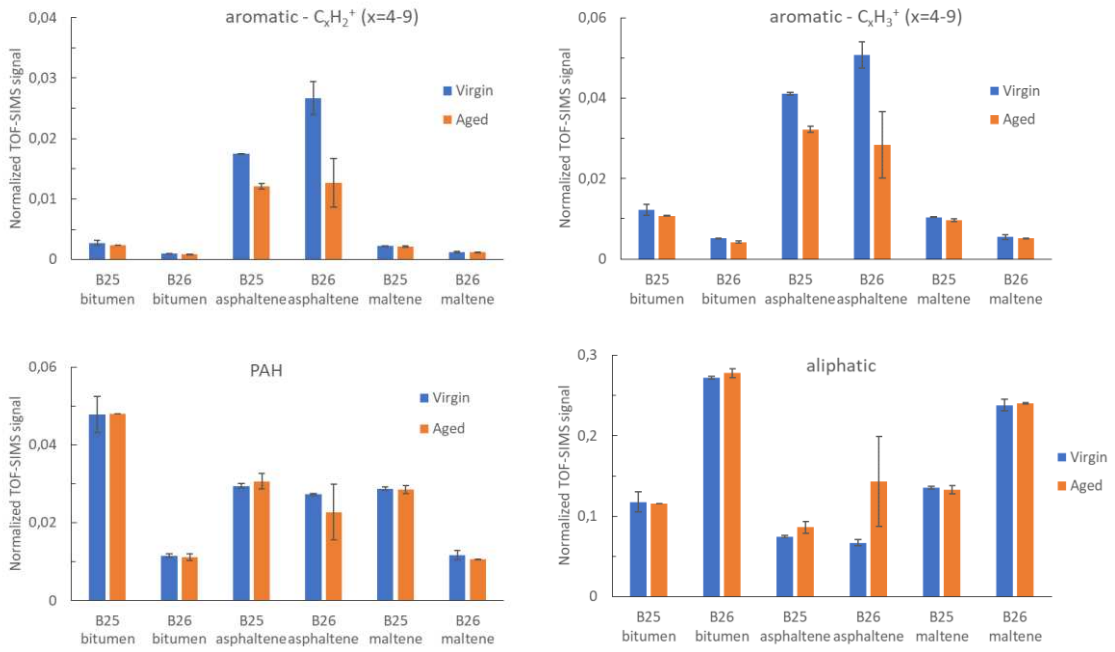

Figure 7. Positive TOF-SIMS signal intensities of aromatic, PAH, and aliphatic ions (PAH: C_9H_7 + $C_{10}H_8$ + $C_{11}H_9$ + $C_{12}H_9$ + $C_{13}H_9$ + $C_{14}H_{10}$ + $C_{15}H_9$ + $C_{16}H_{10}$ + $C_{17}H_{11}$; aliphatic: C_3H_7 + C_4H_9 + C_5H_{11} + C_6H_{13} + C_7H_{13}). The signal intensities are normalized to the total signal intensity of all included ions. The displayed values are means with error bars corresponding to ± 1 standard deviation (n=3).

Signal intensities of selected negative ions are shown in Figure 8. Consistent with the positive ion data, the results indicate that the asphaltenes are more aromatic and less aliphatic as compared to the maltenes. The asphaltenes show higher signal of CN^- ions, whereas organic sulfur (C_nHS^-) is more abundant in the maltenes (B25 only). Furthermore, the maltenes from B26 are more aliphatic but generate less CN^- and C_xHS^- compared to the maltenes from B25. Upon aging, SO_x^- increases significantly, and the increase is larger in the asphaltenes than in the maltenes. This is also in agreement with the FTIR analysis of S=O at 1030 cm^{-1}. Moreover, the effect of bitumen aging on the SO_x^- ions is larger for B25 than for B26, for both the asphaltenes and the maltenes. In contrast to SO_x^-, the effect of aging on the C_xHS^- yield is very small, showing a slight increase for the asphaltenes but a small decrease for the maltenes. For both asphaltenes and maltenes, aging slightly decreases the yields of the aromatic ions and CN^-.

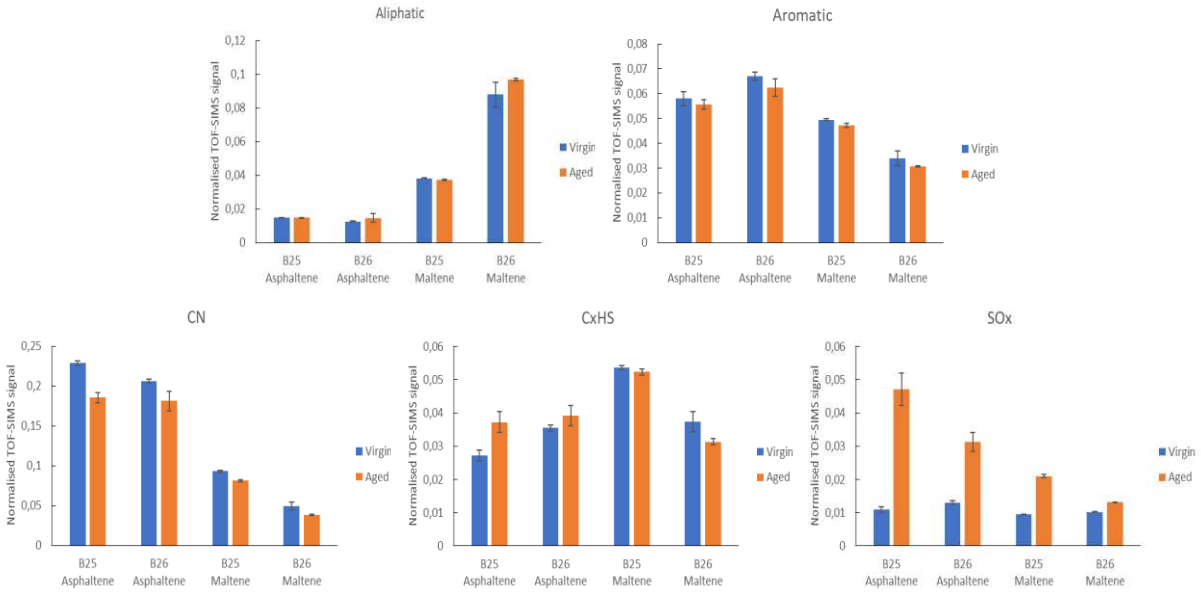

Figure 8. Negative TOF-SIMS signal intensities of selected ions (aliphatic: $C_3H_2 + C_3H_3 + C_4H_3 + C_5H_3$; aromatic: $C_6H + C_{10}H + C_{12}H$; CxHS: $C_2HS + C_4HS + C_6HS + C_8HS$; SOx: $SO_2 + SO_3$). The signal intensities are normalized to the total signal intensity of all included ions (m/z 20-200). The displayed values are means with error bars corresponding to ± 1 standard deviation (n=3).

3.5 GPC

In GPC, the bituminous components are eluted in order of decreasing molecular weight. The obtained chromatograms are shown in Figure 9. For bitumen samples, one can see a fraction of larger molecular weight at retention time of less than about 15 minutes and a fraction with retention time longer than 15 minutes. After aging, the large molecule fraction is increased at the expense of another fraction. As consequence, increases in the molecular weights are observed for the whole bitumen when subjected to aging (Figure 10).

The described large molecular weight fraction of bitumen is often believed to be a part of asphaltenes. This is partly confirmed by the GPC analysis of asphaltene samples. As shown in Figure 8, for B25, the asphaltene fraction are mainly those molecules of shorter retention time (< 15 minutes) or larger molecules. For B26, the asphaltenes also consist of a big portion of larger molecules; however, molecules of lower molecular weight are almost equally significant. In general, the part of smaller molecules mainly contributes to the maltene fraction. But no matter virgin or aged, certain molecular overlaps obviously exist between the maltenes and asphaltenes, as illustrated in Figure 9. This is not surprising since both the fractions are solubility classes which are not only dependent on the molecular weight but also affected by other factors such as polarity

and/or aromaticity of the molecules. This also means that after aging some low molecular weight compounds originally belonging to the maltene fraction may become part of asphaltenes. Consequently, the aged bitumen shows an increase in the molecular weight and an increase in the content of asphaltenes, but the average molecular weight of the asphaltenes is reduced, as illustrated particularly by B25 in Figure 10. According to the FTIR analysis (Cf. Section 3.1), the asphaltenes separated from the aged B25 contain much more polar fractions (carbonyls and sulfoxides) compared to the asphaltenes from the virgin B25, and those polar fractions are probably not large molecules.

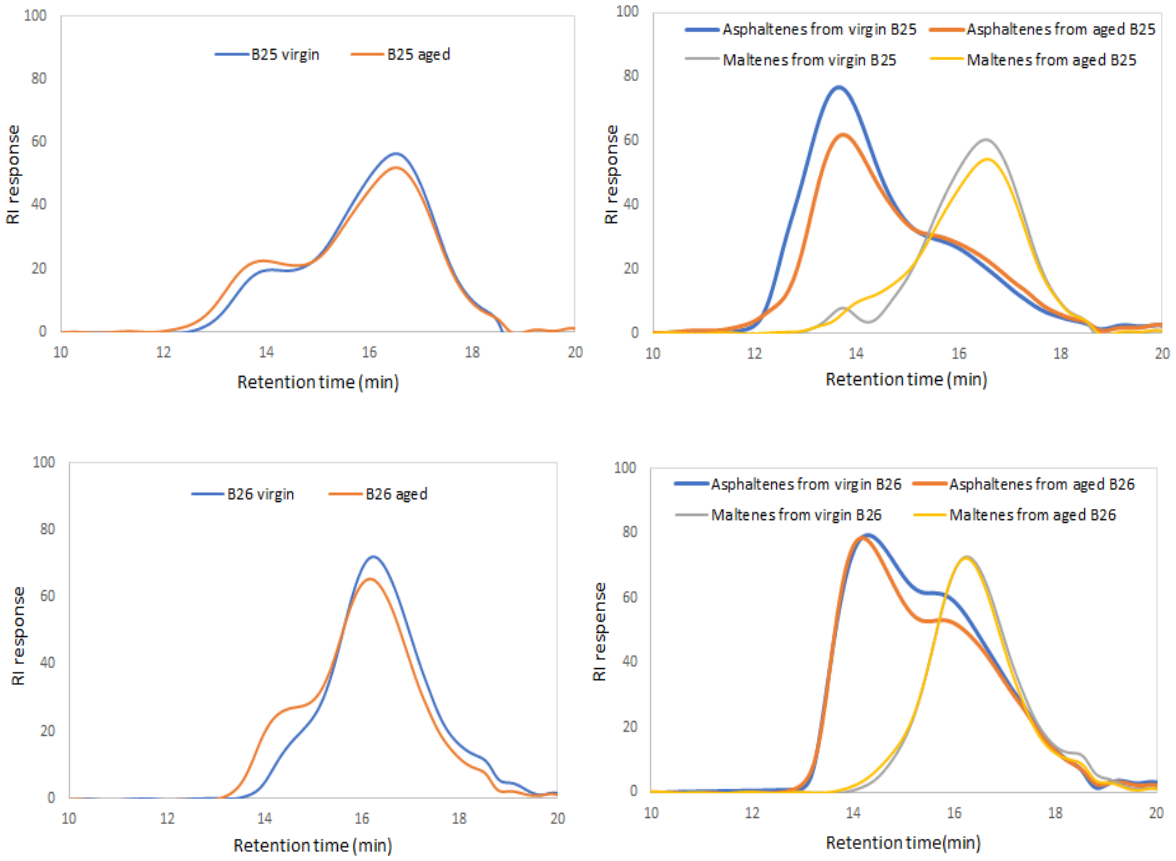

Figure 9. GPC chromatograms of bitumen, asphaltenes, and maltenes before and after aging

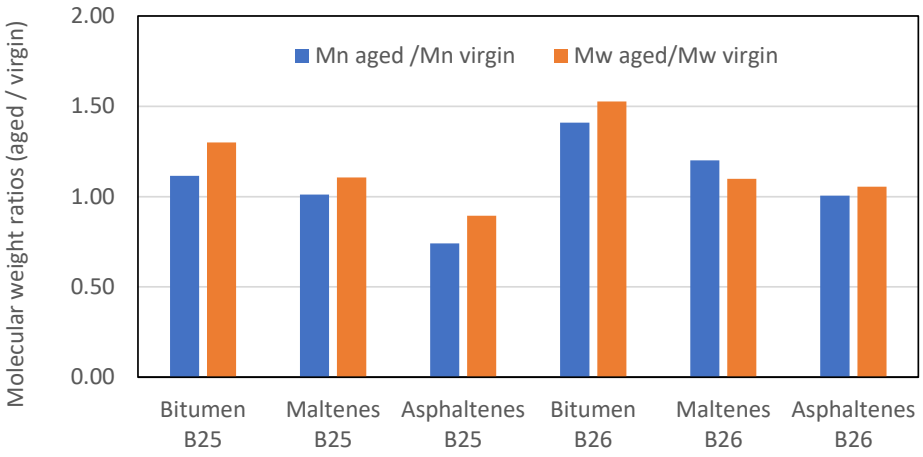

Figure 10. Molecular weight ratios (aged / virgin) of bitumen, asphaltenes and maltenes

4. Conclusions

Asphaltenes and maltenes of two different bitumen (B25 and B26) before and after a laboratory long-term aging are studied by various analytical methods. For comparison, the virgin and aged binders are also analyzed. It has been shown that bitumen B25 is wax-free while B26 contains wax. After fractionation, more wax is found in the maltenes compared to the parent bitumen, and this is even more evident when the bitumen is aged. The bitumen samples also differ in the methyl, α-alkyl and aromatic regions as detected by ^{1}H-NMR; similar differences are also found in the maltene fractions.

In the asphaltenes, the IR signals associated with saturated hydrocarbons are different from those in the bitumen and maltenes. For one bitumen (B26), asphaltenes from the virgin binder do not contain carbonyls, and these all fall into the maltene fraction. After aging of the bitumen, a large part of the carbonyl and sulfoxide signals is found in the asphaltene fraction, suggesting that a lot of molecules become insoluble in n-heptane after reaction with oxygen to form carbonyl and sulfoxide groups. This explains the increase of the more polar fractions in asphaltenes due to aging, also results in the molecular weight changes measured by GPC. For aromaticity, differences are evidenced as: asphaltenes > bitumen > maltenes; after bitumen aging, aromaticity is increased in asphaltenes but not in maltenes. For the whole binders, as expected, aging increases carbonyls and sulfoxides, and there is a minor increase in aromaticity.

TOF-SIMS shows that maltenes are close to the corresponding bitumen, but asphaltenes are more different. It is also shown that maltenes are relatively unaffected by aging while larger differences

are found in the asphaltenes between the virgin and aged bitumen. In general, asphaltenes are more aromatic and less aliphatic than the bitumen and maltenes. Upon aging of the bitumen, asphaltenes show a decrease in aromatic ions and an increase in aliphatic ions. Moreover, when the binders are aged, SO_x are increased significantly, especially in the asphaltenes. This somewhat agrees with the FTIR analysis of sulfoxides. However, it is unable to track changes in carbonyls by using TOF-SIMS.

Considering molecular weight, large molecular weight fraction of bitumen is mainly part of the asphaltenes. However, asphaltenes also contain molecules of lower molecular weight that overlap with maltenes, since these solubility classes are not only dependent on the molecular weight but also affected by the polarity and/or aromaticity of the molecules. GPC analysis also shows that upon aging some low molecular weight compounds become part of the asphaltenes, most probably because of the increased polar fractions as confirmed by FTIR. This indicates that the aged binders display increased contents of asphaltenes and increased molecular weights, but the average molecular weight of the asphaltenes can be reduced after bitumen aging.

References

[1] ASTM D 3279. Standard Test Method for n-Heptane Insolubles.

[2] ASTM D 4124. Standard test methods for separation of asphalt into four fractions.

[3] IP 143, Determination of asphaltenes (heptane insolubles) in crude petroleum and petroleum products.

[4] lP 469. Determination of saturated, aromatic and polar compounds in petroleum products by thin layer chromatography and flame ionization detection.

[5] Redelius R, Soenen H. Relation between bitumen chemistry and performance. Fuel 2015; 140: 34-43.

[6] Mullins OC. The asphaltenes. The Annual Review of Analytical Chemistry 2011; 4: 393-418.

[7] Calandra P, Caputo P, De Santo MP, Todaro L, Turco Liveri V, Oliviero Rossi C. Effect of additives on the structural organization of asphaltene aggregates in bitumen. Construction and Building Materials 2019; 199: 288-297.

[8] Painter P, Veytsman B, Youtcheff J. Phase behavior of bituminous materials. Energy and Fuels 2015; 29 (11): 7048-7057.

[9] Chailleux E, Queffélec C, Borghol I, Farcas F, Marceau S, Bujoli B. Bitumen fractionation: Contribution of the individual fractions to the mechanical behavior of road binders. Construction and Building Materials 2021; 271, art. no. 121528.

[10] Chacón-Patinõ ML, Smith DF, Hendrickson CL, Marshall AG, Rodgers RP. Advances in Asphaltene Petroleomics. Part 4. Compositional Trends of Solubility Subfractions Reveal that Polyfunctional Oxygen-Containing Compounds Drive Asphaltene Chemistry. Energy and Fuels 2020; DOI: 10.1021/acs.energyfuels.9b04288

[11] Nellensteyn FJ. The constitution of asphalt. Journal of the Institute of Petroleum Technology 1924; 10: 311–325.

[12] Pfeiffer JP, Saal RNJ. Asphaltic bitumen as colloidal system. Journal of Physical Chemistry 1940; 44: 139-49.

[13] Marvillet J. Influence of asphalt composition on its rheological behavior. Proc. Association of Asphalt Paving Technologists 1975; 44: 416-443.

[14] Saal RNJ, Labout JWA. Rheological properties of asphaltic bitumens. J. Phys. Chem. 1940; 44: 149-165.

[15] Gokhman LM, Gurary EM. Investigation of rheological and physico-mechanical properties of structure-formation components of road bitumens. Fuel Science and Technology International 1993; 11: 397-401.

[16] Lesueur D. The colloidal structure of bitumen: Consequence on the rheology and on the mechanisms of bitumen modification. Advances in Colloid and Interface Science 2009; 145: 42-82.

[17] Corbett LW. Relationship between composition and physical properties of asphalt. Proc. Association of Asphalt Paving Technologists 1970; 39: 481.

[18] Petersen JC. A Review of the Fundamentals of Asphalt Oxidation (E-C140). Transp. Res. Rec. J. Transp. Res. Board. (2009). https://doi.org/10.17226/23002.

[19] Yu X, Burnham NA, Granados-Focil S, Tao M. Bitumen's microstructures are correlated with its bulk thermal and rheological properties. Fuel 2019; 254, art. no. 115509, DOI: 10.1016/j.fuel.2019.05.092

[20] Poirier MA, Sawatzky H. Changes in chemical component type composition and effect on rheological properties of asphalts. Preprints of Symposium: Chemistry and Characterization of Asphalts, Division of Petroleum Chemistry, American Chemistry Society, 1990, 35: 301-307.

[21] Thenoux G, Bell CA, Wilson JE. Evaluation of physical and fractional properties of asphalt and their interrelationship. Transportation Research Record 1988; 1171: 82-97.

[22] Loeber L, Muller G, Morel J, Sutton O. Bitumen in colloid science: A chemical, structural and rheological approach. Fuel 1998; 77 (13): 1443-1450.

[23] Hofko B, Eberhardsteiner L, Füssl J, Grothe H, Handle F, Hospodka M, Grossegger D, Nahar SN, Schmets AJM, Scarpas A. Impact of maltene and asphaltene fraction on mechanical behavior and microstructure of bitumen. Materials and Structures 2016; 49 (3): 829-841.

[24] Weigel S, Stephan D. Relationships between the chemistry and the physical properties of bitumen. Road Materials and Pavement Design 2018; 19 (7): 1636-1650.

[25] Ghasemirad A, Bala N, Hashemian L. High-temperature performance evaluation of asphaltenes-modified asphalt binders. Molecules 2020; 25 (15), art. no. 3326. DOI: 10.3390/molecules25153326

[26] Wang C, Xie W, Underwood BS. Fatigue and healing performance assessment of asphalt binder from rheological and chemical characteristics. Materials and Structures 2018; 51 (6), art. no. 171. DOI: 10.1617/s11527-018-1300-2

[27] Pauli AT, Branthaver JF. Relationships between asphaltenes, heithaus compatibility parameters, and asphalt viscosity. Petroleum Science and Technology 1998; 16 (9-10): 1125-1147.

[28] Mirwald J, Werkovits S, Camargo I, Maschauer D, Hofko B, Grothe H. Understanding bitumen ageing by investigation of its polarity fractions. Construction and Building Materials 2020; 250: 118809.

[29] Mirwald J, Werkovits S, Camargo I, Maschauer D, Hofko B, Grothe H. Investigating bitumen long-term-ageing in the laboratory by spectroscopic analysis of the SARA fractions. Construction and Building Materials 2020; 258: 119577.

[30] Boysen RB, Schabron JF. The automated asphaltene determinator coupled with saturates, aromatics, and resins separation for petroleum residua characterization. Energy Fuels 2013; 27:4654-4661.

[31] Adams JJ, Elwardany MD, Planche JP, Boysen RB, Rovani JF. Diagnostic techniques for various asphalt refining and modification methods. Energy Fuels 2019; 33: 2680-2698.

[32] Lin MS, Davison RR, Glover CJ, Bullin JA. Effects of asphaltenes on asphalt recycling and aging. Transportation Research Record 1995; 1507: 86-95.

[33] Elkashef M, Elwardany MD, Liang Y, Jones D, Harvey J, Bolton ND, Planche J-P. Effect of using rejuvenators on the chemical, thermal, and rheological properties of asphalt binders. Energy and Fuels 2020; 34 (2): 2152-2159.

[34] Fini E, Rajib AI, Oldham D, Samieadel A, Hosseinnezhad S. Role of chemical composition of recycling agents in their interactions with oxidized asphaltene molecules. Journal of Materials in Civil Engineering 2020; 32 (9), art. no. 04020268. DOI: 10.1061/(ASCE)MT.1943-5533.0003352

[35] Lu X, Sjövall P, Soenen H, Blom J, Makowska M. Oxidative aging of bitumen: a structural and chemical investigation. Road Materials and Pavement Design 2021; DOI: 10.1080/14680629.2021.1871936

[36] EN 12607-1. Bitumen and bituminous binders. Determination of the resistance to hardening under influence of heat and air – Part 1 RTFOT method.

[37] EN 14769. Bitumen and bituminous binders - Accelerated long-term ageing conditioning by a Pressure Ageing Vessel (PAV).

[38] ASTM D 5291. Standard test methods for instrumental determination of carbon, hydrogen, and nitrogen in petroleum products and lubricants.

[39] DIN 51595. Determination of asphaltene content of petroleum products by precipitation in heptane.

[40] Claudy P, Letoffe JM, King GN, Plancke JP. Characterization of asphalts cements by thermomicroscopy and differential scanning calorimetry: correlation to classic physical properties. Fuel Science and Technology International 1992; 10 (4-6): 735-765.

[41] Michon LC, Netzel DA, Turner TF, Martin D, Planche JP. A 13C NMR and DSC study of the amorphous and crystalline phases in asphalts. Energy Fuels 1999; 13(3): 602-610.

[42] Lu X, Langton M, Olofsson P, Redelius P. Wax morphology in bitumen. Journal of Materials Science 2005; 40: 1983-1900.

[43] Lu X, Redelius P. Compositional and structural characterization of waxes isolated from bitumens. Energy Fuels 2006; 20: 653-660.

[44] Hofko B, Alavi MZ, Grothe H, Jones D, Harvey J. Repeatability and sensitivity of FTIR ATR spectral analysis methods for bituminous binders. Materials and Structures 2017; 50: 187.

[45] Rossi CO, Caputo P, De Luca G, Maiuolo L, Eskandarsefat S, Sangiorgi C. 1H-NMR spectroscopy: a possible approach to advanced bitumen characterization for industrial and paving applications, Appl. Sci. 2018; 8 (2): 229.

[46] Lu X, Sjövall P, Soenen H. Structural and chemical analysis of bitumen using time-of-flight secondary ion mass spectrometry (TOF-SIMS). Fuel 2017; 199: 206-218.

[47] Sjövall P, Pomerantz AE, Lu X, Mullins OC. Time of flight – secondary ion mass spectrometry (TOF-SIMS) study of diverse asphaltenes. Fuel 2018; 220: 638-644.

[48] Stephan T, Jessberger EK, Heiss CH, Rost D. TOF-SIMS analysis of polycyclic aromatic hydrocarbons in Allan Hills 84001. Meteoritics & Planetary Science 2003; 38: 109–116.

[49] Sjövall P, Bake KD, Pomerantz AE, Lu X, Mitra-Kirtley S, Mullins OC. Analysis of kerogens and model compounds by time-of-flight secondary ion mass spectrometry (TOF-SIMS). Fuel 2021; 286: 119373.